

Ion-kinetic-energy sampling in a 22-pole trap using ring-electrode evaporation

Miguel Jiménez-Redondo,^{1,*} Dieter Gerlich,^{1,2} Paola Caselli,¹ and Pavol Jusko¹

¹Max Planck Institute for Extraterrestrial Physics, Gießenbachstraße 1, 85748 Garching, Germany

²Department of Physics, Technische Universität Chemnitz, 09107 Chemnitz, Germany

(Dated: January 30, 2025)

We present an experimental method for the characterization of the kinetic energies of ions confined in a 22-pole radio frequency trap by inducing a small potential barrier using the surrounding ring electrodes, allowing the selective extraction of ions. Energy sampling experiments have been performed on buffer gas thermalized He⁺ ions at trap temperatures between 10 – 180 K, resulting in distinct extraction curves as a function of the potential barrier, and a differentiated behavior depending on the escape time from the trap. The experiments are complemented by Monte Carlo simulations of the ion trajectories inside the calculated trap potential and allow us to investigate the properties of the sampling method, the role of ion motion coupling, and the impact of residual buffer gas collisions on the observed results. The technique has also been successfully applied to identify energetic H₃⁺ ions produced in an exothermic reaction inside the trap. Upon calibration, this method can provide relative kinetic energy distributions or be used to filter the maximum desired kinetic energy of the ions inside the trap.

I. INTRODUCTION

Radio frequency (rf) ion traps are useful tools for the study of ion-molecule processes. The combination of high-order multipole ion traps, providing large field-free trapping regions, with cryogenic cooling allows the study of such processes at temperatures relevant for interstellar chemistry. A careful determination of the temperature, or more generally, the energy distribution of the trapped ions, is crucial in order to accurately characterize the studied process. Furthermore, insight on the energies of the trapped ions can potentially help with identification of the trapped species, allowing for the differentiation of isomers or internally excited species.

The measurement of the temperature of the ion ensemble is commonly sufficient to characterize the ion energies. Thermometry techniques for ion traps include the use of rotational spectroscopy to determine the rotational temperature and using the Doppler broadening of the lines to obtain the translational temperature, using photodetachment [1–3], laser induced reaction [4] or rare gas tagging [5] action schemes. Time-of-flight distributions have also been proposed as a method for temperature determination [6]. In magneto-optical traps (MOT), the temperature of the atoms has been derived from the free expansion of the ion cloud [7], and a more precise determination of the energy distribution has been obtained by coupling a single atom standing-wave dipole trap to the MOT [8].

Energetic characterization of photodissociation processes has been tackled with velocity map imaging setups. These have been successfully coupled to cylindrical [9] and Paul [10] traps in order to determine the kinetic energy of the photodissociation fragments.

Some works have dealt with the use of electrostatic

potentials for energy characterization in traps. Champeau *et al.* [11] used a retarding potential to discriminate ions according to their energy after their extraction from a quadrupole ion trap and contrasted the results with their time-of-flight measurements. Evaporative techniques, based on the use of a potential barrier to selectively extract ions according to their energy, have been used to characterize the ions in 22-pole trap experiments. These methods can be used to sample the energy distribution of the ions along the different trap axes, and unlike time-of-flight measurements, can selectively preserve the low energy ions in the trap for further experiments. Lakhmanskaya *et al.* [12] studied the evaporative ion losses in a 22-pole trap in the radial and axial directions by regulating the trap temperature and end cap voltage, and used the loss rate to derive the ion temperature. This sort of technique is also used in the recently developed leak-out spectroscopy (LOS) method [13], which uses vibrational to translational energy transfer to generate energetic ions capable of escaping through the end cap potential. Forced evaporative cooling has also been successfully applied to negatively charged particles both in the context of antimatter research [14], by cooling antiprotons down to 9 K; and for molecular anions in an octopole trap [15], where it is demonstrated to be more effective than buffer-gas cooling.

The question of the ion energy distribution in multipole traps has also been approached from a computational point of view, usually with an emphasis on buffer gas cooling and the effect of the micromotion induced by the rf field in the final energy distribution [16–20]. Particularly, the effect of end cap voltage and buffer gas mass has been investigated using Monte Carlo simulations of the ion trajectories in 22 pole [17] and 16 pole and 16 wire [18] traps. Trajectory simulations have also been used to model the trapping process and the resulting energies in a ring electrode trap without the use of buffer gas [21]. In the μK regime, the limits of buffer gas cooling of atomic ions in Coulomb crystals have been

* mjimenez@mpe.mpg.de

explored for Paul traps [22] and then extended to several trap geometries including multipoles [23].

In this work, we present an experimental method for the characterization of the kinetic energy distribution of ions inside a 22-pole trap. The small the potential barrier generated by a surrounding ring electrode, which allows for finer control over the energy of the ions compared to the end cap voltage, is used to discriminate the ions according to their energy.

This setup is used to characterize thermalized He^+ ions at different trap temperatures. Monte Carlo simulations of the ion trajectories under energy sampling conditions are used to reproduce the experimental data and support the interpretation of the experimental results. The method is also applied to H_3^+ ions produced inside the trap in an exothermic reaction, highlighting the potential to selectively sample energetic ions.

II. EXPERIMENTAL SETUP

The experimental setup has been previously described in detail in [24]. It consists of a 22-pole trap (5 cm long, 1 cm diameter) with stainless steel rods (1 mm diameter) surrounded by five ring electrodes. The trap is mounted on top of a helium cryostat which allows the cooling of the device down to 4 K. A heater cartridge is used to set the desired temperature which is measured using silicon diodes placed on the trap enclosure. The trap temperature can be determined with an accuracy of ± 1 K in this way. The pressure in the trap vacuum chamber is monitored using a Bayard-Alpert gauge calibrated by a capacitance manometer directly connected to the trap volume. This setup can measure pressures down to $\sim 10^{-8}$ mbar inside the trap, but cannot be reliably used to monitor changes over short timescales, such as the He buffer gas pulse used in the experiments.

He^+ ions are produced in a Gerlich type Storage Ion Source (SIS) [25] by electron bombardment of neutral He, and are subsequently guided through a quadrupole acting as a mass filter and an electrostatic bender before arriving into the trap. A short (24 ms) and intense He pulse, injected through a custom piezo-element actuated valve, is used to slow down the ion beam which allows efficient trapping of the ions. This He also acts as a buffer cooling gas, allowing the ions to cool down to a temperature close to the one of the trap. After the desired trapping time, ions are released to a second quadrupole allowing the m/z characterization by mass spectrometry and subsequently detected using a conversion dynode together with a channel electron multiplier. A multi-channel scaler (MCS) enables resolving the time of arrival of the ions at the detector.

During each 2 s energy sampling experiment, the trap alternates between two different configurations in which only the voltage applied to the exit electrode, SA, changes. For the full duration of the cycle, the ring electrode R4 (the second closest to the trap exit) is set to

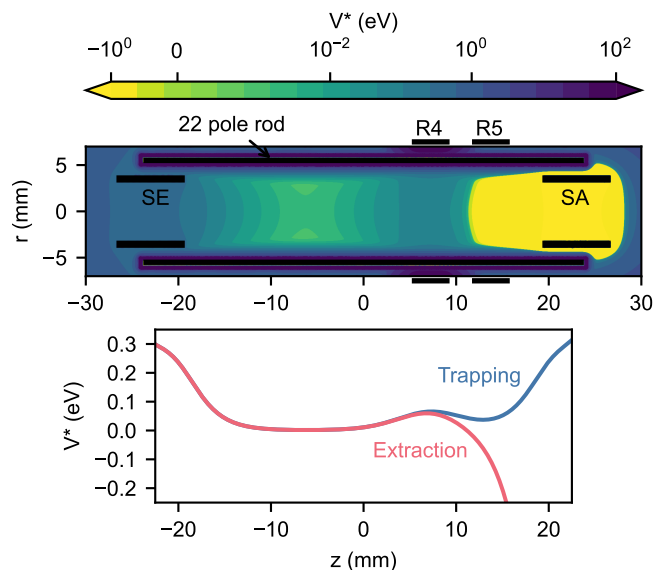


FIG. 1. (Color online) Top panel: cut through the calculated effective mechanical potential inside the 22-pole trap (rz) set for the extraction configuration of the energy sampling experiment. The frequency and amplitude of the rf voltage applied to the 22 poles are $f_0 = 19$ MHz and $V_0 = 57$ V. The voltages for the entrance, exit and ring electrodes are $V_{SE} = 0.3$ V, $V_{SA} = -1.5$ V and $V_{R4} = 80$ V respectively. The corresponding ring electrode barrier height, V_{R4}^* , is 58.6 meV. Bottom panel: effective mechanical potential calculated on the trap axis for the configurations employed in the experiments when trapping (blue) and extracting (red) the ions. Electrode voltages are the same as in the top panel, $V_{SA} = 0.3$ V for the trapping configuration.

a voltage V_{R4} between 0 and +147 V, creating a small ($\sim 1 : 1000$ ratio) barrier inside the trap. During loading of the trap (30 ms) and the subsequent 1 s trapping time, the exit electrode SA is kept at a positive value (0.3 V) in order to ensure the storage of the ions. This is referred to hereafter as the trapping configuration. The 1 s trapping time ensures ions have enough time to cool down and allows the neutral He buffer gas (pulsed into the trap in the few first ms of the sequence) to be evacuated. After this storage time, the SA electrode is set for extraction, i. e., to negative voltage (-1.5 V), such that it allows the ions with sufficient energy to overcome the R4 barrier and be guided out of the trap towards the detector. The escaped ions are counted in a time-resolved manner (MCS) in a 300 ms interval following the opening of the SA electrode. Each experiment is repeated 60 times in order to obtain a good signal over the whole detection interval. The calculated effective mechanical potential V^* inside the trap for both configurations is depicted in Fig. 1.

The extraction potential created by SA can distort the potential barrier created by the ring electrodes, making the ring electrode closest to the trap exit, R5, a poor choice for energy sampling experiments. Therefore, as we have previously described, we chose to use the next

ring electrode, R4, instead [24]. Moreover, the influence of SA is still relevant for the lower R4 voltages employed, requiring careful examination of this effect for the energy characterization of the ions. The simulations also showed that the barrier has a radial profile with the minimum value at the axis of the trap, which possibly affects the sampling of the ions [24]. In any case, when discussing the potential barrier, we always refer to its value at the axis, noted by V_{R4}^* , throughout this work.

III. SIMULATIONS

In order to interpret the experimental results, we performed Monte Carlo simulations of a number of ions (usually 1000) moving inside the given trap potential and potentially colliding with buffer gas atoms. The trajectory of each ion is solved until either the ion reaches the exit electrode SA or a total of 100 ms are elapsed. These simulations were performed for varying values of the ion temperature (or buffer gas temperature, see below), buffer gas pressure and R4 voltage.

It is critical in these simulations to get an accurate reproduction of the individual ion energetics as it moves inside the trap. Most standard integration methods struggle with energy conservation, as the total ion energy slowly drifts, usually to higher values. Therefore, we have used the velocity Verlet algorithm [26], belonging to the family of symplectic methods which ensure low energy drift over extended simulation times [27], to solve the ion trajectories. A second important factor is the treatment of the field governing the ion motion. We adopt the effective mechanical potential V^* , from the Boundary Element Method (BEM) calculations [28, 29] using a 3D mesh of the trap generated with the Salome platform [30] (cf. [24] for further details), to solve the ion trajectories, given that the macromotion of the ions is controlled by V^* . This is useful for easier visualization of the general properties of ion motion inside the trap. For most of the simulations, however, a time-dependent rf field has been employed. In this case, the electric field for an ideal multipole [25]

$$\begin{pmatrix} E_x \\ E_y \end{pmatrix} = \frac{V_0}{r_0} n \left(\frac{r}{r_0} \right)^{n-1} \begin{pmatrix} -\cos(n-1)\varphi \\ \sin(n-1)\varphi \end{pmatrix} \cos \Omega t \quad (1)$$

where r and φ are the polar coordinates, r_0 is the inscribed radius, $n = 11$ is the multipole order, and V_0 and $\Omega = 2\pi f_0$ are the amplitude and angular frequency of the time-dependent rf voltage applied to the 22 poles respectively, has been superimposed to the electrostatic contribution of the end and ring electrodes from the BEM simulations. Attempting to use the BEM calculated rf field instead resulted in unstable trajectories likely due to numerical artifacts in low potential regions.

The individual ion trajectories are solved using a fixed time step (required by the symplectic algorithm) that is chosen at the start of the simulation based on the total

ion energy and recalculated if the energy changes due to a collision. This step is chosen as large as possible for computational efficiency while still ensuring that energy is conserved through the trajectory, and is of the order of ns (in comparison the rf period is 52 ns). At fixed times during the simulation, namely every μs , a check is performed on whether the ion has escaped the trap, the trajectory data is saved, conservation of energy is tested and the probability of an elastic collision of the ion with the buffer gas is checked using the Langevin cross section. In case a collision occurs, the outcome is determined following Londry *et al.* [31], generating a random scattered direction for the ion and a random Maxwellian velocity for the neutral and calculating the resulting ion velocity. Ions are considered to have escaped from the trap when they reach the axial coordinate of the exit electrode SA ($z = 20$ mm). The exit time recorded is the time needed to reach this position, since the focusing and detection of the ions is not simulated. The flight time between leaving the trap (SA) and detection event in the experiment is negligible on these time scales. Nevertheless, the configuration of the ring electrode could potentially affect the experimental focusing of the ions and change the detection efficiency. A careful treatment of this effect would require extending the simulation of the ion trajectories up to the detector and is out of the scope of this work, but needs to be considered when comparing experimental and simulation results.

The velocity distribution of ions collisionally cooled by a buffer gas in a 22-pole trap diverges from a Maxwell-Boltzmann distribution due to the potential of the trap, which leads to the depletion of the low energy region of the distribution, and the ‘rf heating’ effect caused by collisions with the buffer gas particles in regions with a strong rf field [17]. A Tsallis distribution [32] is commonly used to empirically fit the resulting energy distribution [6, 16]. Thus, in order to obtain a good initial energy distribution, the simulation of the experiment is divided in two steps. In the first one, ions are cooled down from room temperature by collisions with 10^{-4} mbar of buffer gas during 100 ms, which is sufficient to ensure thermalization, keeping the exit electrode closed. After the simulation is done, the resulting final velocities and positions of the ions are used as initial conditions for the extraction simulation, where the voltage applied to the SA electrode is switched to a negative value. For simplicity, we will simply refer to these conditions throughout the text as “ions at temperature T ”, where T is the temperature of the buffer gas in the corresponding cooling simulation.

IV. RESULTS AND DISCUSSION

The experimental data is obtained as time-resolved histograms of the ions arriving at the detector. Two examples of this are given in Fig. 2. Typically, a large fraction of the ions arrive within a few ms of the trap opening

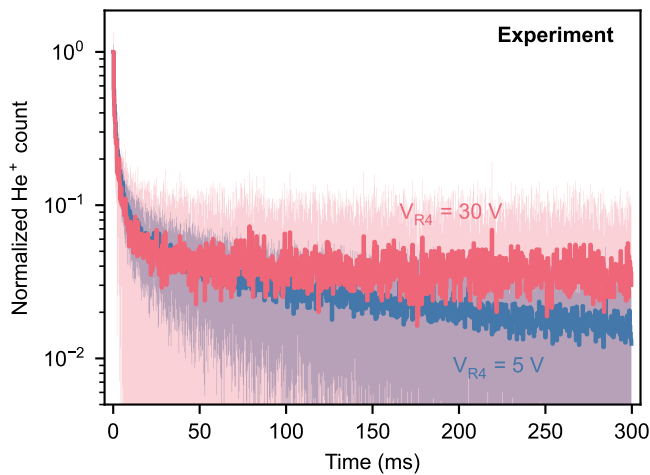


FIG. 2. Time of arrival of He^+ ions at the detector for a trap temperature of 36 K and two different voltages of the R4 ring electrode. Shaded areas represent the uncertainty in the measurement. Values are normalized to the maximum for comparison.

(switching the SA voltage from +0.3 to -1.5 V), and the signal decays sharply and stabilizes after ~ 10 ms to a value between $\sim 1 - 10\%$, depending on the particular V_{R4} voltage and trap temperature. From that point on to the end of the measurement at 300 ms, a roughly constant countrate is observed. An exception to this is found at very low V_{R4} voltages, where the trap is significantly depleted over the 300 ms measurement and therefore an exponential decay trend is observed for the longer timescales, as illustrated by the $V_{R4} = 5$ V measurement in that figure. These two markedly different behaviors at short and long timescales hint at two different mechanisms through which the ions can escape the trap. For this reason, we have chosen to process the experimental results in two ways, by integrating the time-resolved measurements in full or only for the first ms.

The experimental results of the energy sampling measurements are shown in Fig. 3. The ion signal after opening the exit electrode was recorded for different trap temperatures and ring electrode voltages and then integrated in the aforementioned two ways.

The 300 ms integration time results in a slow decay of the ion signal as the ring electrode voltage is increased. A small plateau in the very first V_{R4} voltages (up to ~ 10 V for the 180 K data) is followed by a decay that is dependent on the ion temperature, although the data for 17 and 36 K present very similar behaviors. Full trapping can be achieved at $V_{R4} = 75$ V for the two lowest temperatures. At the maximum available ring electrode voltage, 147 V, ions are effectively trapped for all except the 180 K experiment, in which $\sim 5\%$ of the ions are still able to escape over the barrier.

Reducing the integration time to 1 ms results in a notable change in the shape of the curves. A steady drop is now present from the beginning, and the signal de-

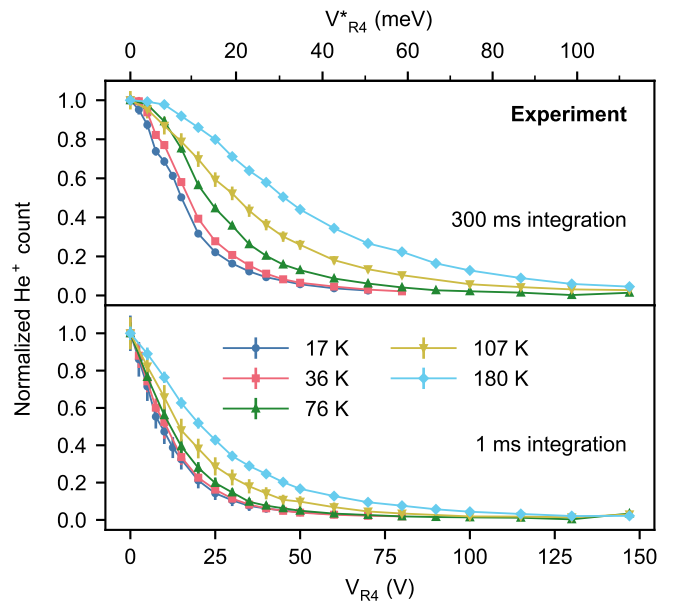


FIG. 3. He^+ ions extracted as a function of the voltage applied to the R4 ring electrode for different trap temperatures. Upper panel: 300 ms integration time. Lower panel: 1 ms integration time. Top axis shows the calculated potential barrier for each R4 voltage. Ion count is normalized to the maximum for each curve, which corresponds to $V_{R4} = 0$.

cays faster with increasing ring electrode voltage. On the other hand, much smaller differences are observed for the curves at different temperatures, particularly for the data of 76 K and below. Even with the faster decay, the ions are still effectively trapped at similar voltages as in the 300 ms integration time.

To better understand the way ions are behaving inside the trap and the exact conditions that allow them to escape, we can look at the results from the ion trajectory simulations. The first question to address is the correlation between the energy of the ions and their likelihood to escape from the trap. Figure 4 depicts the total energy (E_{total} , sum of kinetic and potential) and axial kinetic energy ($E_{k,z}$) distribution of a simulation of ions at 100 K, showing which ones are able to escape the trap. As expected, no ion with a total energy below the barrier value is extracted, but on the other hand ions with energies 3–4 times higher than the ring electrode barrier remain trapped. Conversely, looking at the axial kinetic energy distribution, ions with $E_{k,z}$ larger than the barrier are almost guaranteed to exit the trap. However, in the full 100 ms simulation, a significant fraction of the ions with $E_{k,z}$ below the barrier are also able to escape. A better correlation can be obtained by only considering the results after the first ms of the simulation. In this case, most of the ions with axial kinetic energy below the barrier remain trapped, while most of the higher energy ones are still extracted.

A more detailed look at the time dependence of the extraction is shown in Fig. 5. Here, the different colors for

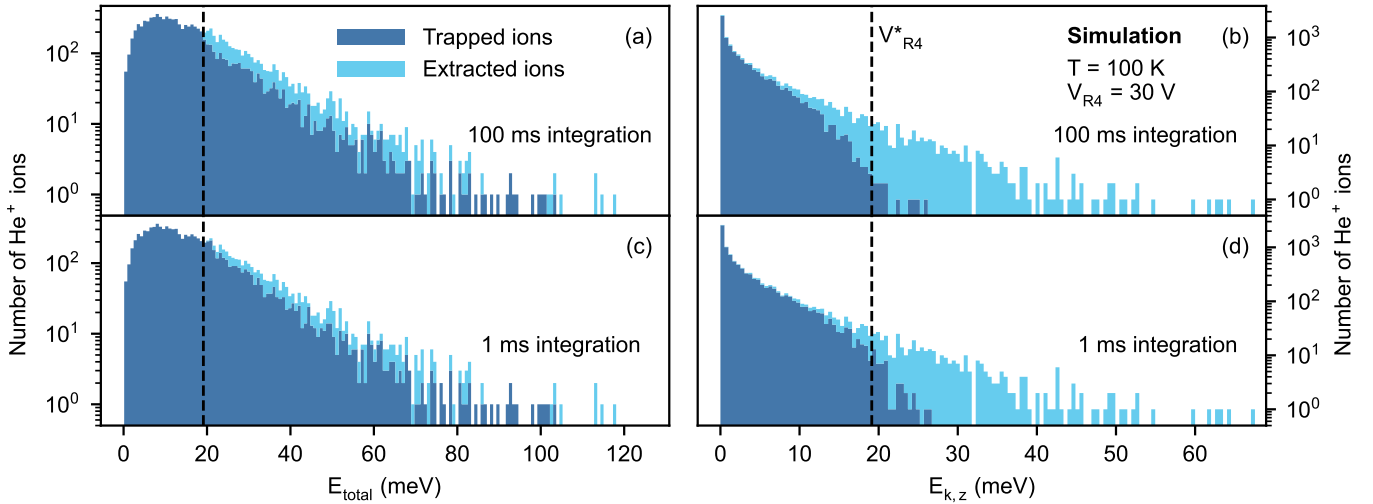


FIG. 4. (Color online) Distribution of trapped (blue) and extracted (cyan, stacked on top) ions according to the initial values of their total (panels (a) and (c)) and axial kinetic (panels (b) and (d)) energies, for 10000 ions at 100 K and $V_{R4} = 30$ V. Dashed black lines indicate the value of the mechanical potential barrier. Top panels: results after the full 100 ms simulation. Bottom panels: results after 1 ms.

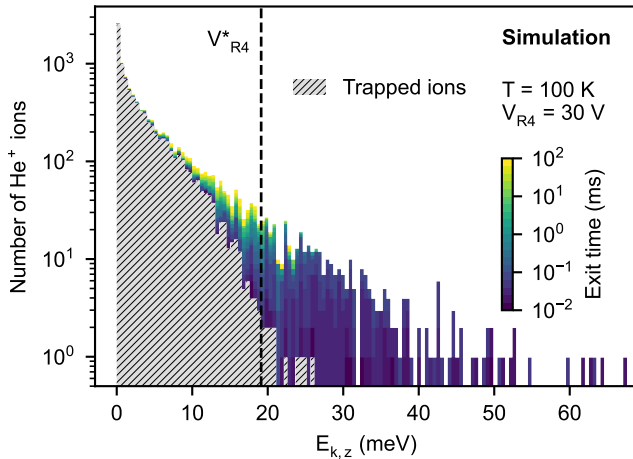


FIG. 5. (Color online) Initial axial kinetic energy distribution for the same conditions as Fig. 4. Extracted ions are now color-coded as a function of the time needed to exit the trap. The hatch pattern represents the fraction of ions that do not escape the trap.

the extracted ions correspond to the time elapsed from the beginning of the simulation until they reach the exit electrode SA. As can be seen, most of the ions with initial axial kinetic energies higher than the barrier need very little time ($\lesssim 0.1$ ms) to exit the trap. At energies lower than V_{R4}^* , times grow to the scale of ms and a significant fraction (note the logarithmic scale) of the ions require close to the full simulation time to be able to escape. As a reference, $\sim 10\%$ of all ions that leave the trap do so after 50 ms. The fact that ions with $E_k < V_{R4}^*$ can still escape the trap is not unexpected, as their initial potential energy might be enough to accelerate them to the needed

velocity, but the long times required by some of them to reach the exit point towards an inefficient exchange of energy between the axial and radial/angular degrees of freedom causing the axial energy to become higher than the V_{R4}^* barrier at a late point in the simulation. A more detailed look into the particulars of the ion motion inside the trap and how this affects the energy exchange can be found in Appendix A.

The inefficient coupling of the different degrees of freedom effectively results in two different regimes when analyzing the energy sampling, separating the first few ms of sampling from the rest of the acquisition. As was shown in Fig. 2, this is also apparent in the time-resolved detection of the extracted ions. A comparison of the experimental data with the simulated time-resolved extraction of the ions is shown in Fig. 6. In both cases, a large fraction of the ions is able to escape the trap in the first few ms. The experimental signal then decays smoothly and is mostly stabilized to a value around 5% of the initial count. In contrast, the simulations predict a sharper decay after the initial extraction. Very few ions (a fraction 20 times smaller than the experimental value) escape after ~ 20 ms in the simulations with no buffer gas, due to the aforementioned inefficient coupling between the axial and radial motion of the ions. The extraction in this region can however be significantly enhanced by including a small pressure of He buffer gas in the simulations (which might remain in the trap from the initial He pulse in the experiment). Collisions with this residual gas effectively repopulate the high energy tail of the distribution, allowing more ions to overcome the potential barrier. This leads to a factor of ~ 10 increase in the extraction at 100 ms with just 2×10^{-6} mbar of residual buffer gas in the trap. Further increasing the pressure in the simulations leads to increased extraction, such that a significant

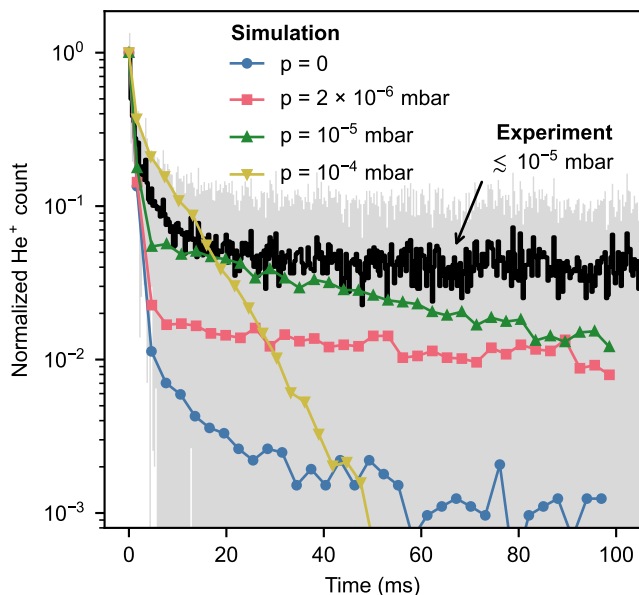


FIG. 6. (Color online) Experimental (bold black line, with uncertainty shaded in gray) and simulated (color lines with symbols) histograms for the extraction times of He^+ ions with a V_{R4} voltage of 30 V. Experiment: time of arrival of the ions at the detector for a trap temperature of 107 K. Simulations: time elapsed from the beginning of the simulation until the ions reach the exit electrode, for ions at 100 K, with different residual buffer gas pressures. Values are normalized to the maximum for comparison.

fraction of the trapped ions are able to escape, leading to the depletion of the trap and an exponential decay of the He^+ count with time. This can be clearly observed in the 10^{-4} mbar simulation.

As mentioned in the experimental section, the time evolution of the pressure inside the trap during the experiments is not reliably resolved by the pressure gauges. Nevertheless, the manometer readings suggest that similar pressures are attained at the different trap temperatures of this study. For this reason, we use the residual gas pressure instead of number density as a parameter for the trajectory simulations. For illustration, the value used for most of the simulations presented here, 2×10^{-6} mbar, corresponds to $8.4 \times 10^{10} \text{ cm}^{-3}$ at 100 K and $2.2 \times 10^{11} \text{ cm}^{-3}$ at 15 K.

Residual buffer gas can then help explain the observed high extraction at longer timescales, and could also be a reason for the experimentally observed smooth decay at the beginning due to the evacuation of this gas from the trap with time, which is not accounted for in the simulations. Nevertheless, a discrepancy still exists between the pressure needed to account for the signal at longer extraction times and the one that better reproduces the experimental results from Fig. 3 (see also Fig. 7 below).

Panels (a) and (c) of Fig. 7 show the simulated energy sampling experiment for ions at different temperatures, with no residual buffer gas present in the trap. As in

Fig. 3, the two panels show the long-time integrated extraction and the first ms signal respectively. In the case of the simulations, there is only a minor difference between both processing methods, due to the low amount of ions leaving the trap after the initial few ms as seen above. Qualitatively, the extraction curves for the 1 ms integration resemble their experimental counterparts the most, with a sharply decreasing trend for the lower V_{R4} voltages. On the other hand, the experimental curves show a more extended profile, and a smaller separation between the different temperatures, especially below 100 K.

The stark difference between simulation and experiment for the 100 ms integration can be somewhat mitigated by including the effect of buffer gas collisions in the sampling. Panels (b) and (d) of Fig. 7 depict again both integration intervals, but now with a residual gas pressure of 2×10^{-6} mbar. The curves for 100 ms and 1 ms are now well differentiated. In the 100 ms case, the enhanced extraction at longer timescales observed in Fig. 6 translates into smoother curves presenting a plateau for the first few V_{R4} values. This behavior was also observed in the experiments, particularly for the 180 K curve. For higher ring electrode voltages, the extraction, particularly at higher temperatures, is significantly enhanced by the presence of buffer gas. Limiting the sampling to the first ms, however, results in a figure almost identical to the one obtained with no buffer gas in the trap, since buffer gas collisions mainly contribute to the extraction at timescales $\gtrsim 5$ ms.

It should be noted that the value of 2×10^{-6} mbar is only chosen as a reasonable pressure that results in relatively good agreement with the sampling experiments. If the presence of residual gas from the cooling He pulse is actually the cause of the observed experimental behavior, then the pressure inside the trap will change over the extraction interval, and its value will very likely be different for the various trap temperatures studied. Thus, the simulated curves (with 100 ms integration) should only be taken as a qualitative example of the type of changes produced by the presence of residual buffer gas in the trap. Increasing the trapping time, i.e., the time between the He buffer gas pulse and the opening of the exit electrode, would reduce the effect of the residual gas in exchange for an increased measurement time. However, potential applications of this technique, such as the study of exothermic reactions inside the trap (see Fig. 9 below), require a certain amount of neutral gas to be present in the trap, hence, the effect of neutral gas collisions cannot be completely avoided.

A direct comparison of the experimental and simulated extraction curves for three different temperatures can be found in Fig. 8. For the simulations, the results with a residual pressure have been used for the comparison in both panels, since it results in a relatively good agreement for the data with long integration times (300 or 100 ms for experiment and simulation, respectively), while for the 1 ms integration times, the simulations with and without residual gas pressure result in

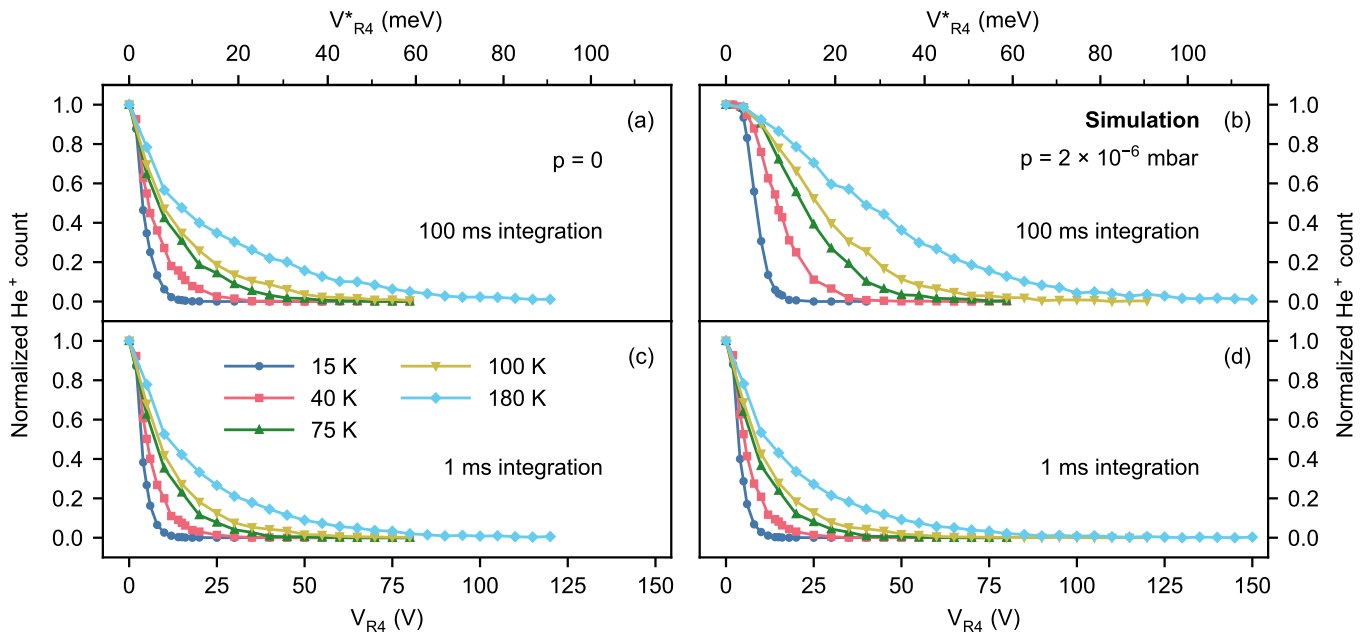


FIG. 7. Simulated number of extracted ions as a function of V_{R4} potential for different trap temperatures, with no residual buffer gas in the trap (panels (a) and (c)) and with a buffer gas pressure of 2×10^{-6} mbar (panels (b) and (d)). Upper panels: fraction of ions extracted in the full 100 ms simulation. Lower panels: fraction of ions that escape the trap in the first ms.

virtually the same curve. For long integration times, the simulation results show a reasonable agreement with the experiments, particularly at the higher temperatures. At 180 K, the simulated curve follows the experimental data quite closely, but always results in an underestimation of about 10% of the fraction of extracted ions. The agreement worsens at lower temperatures. At 40 K, the simulations deviate from the experiments for $V_{R4} > 20$ V, and the 15 K simulation significantly falls significantly below the experimental results. The discrepancy increases for the data with 1 ms integration time, where the simulations always predict much narrower curves than what is observed experimentally. Further details on the differences between the experimental and simulated results are presented in Appendix B. The experimentally enhanced extraction of ions for high V_{R4} voltages was also observed by Lakhmanskaya *et al.* [12] in their evaporation study in a 22-pole trap with constant buffer gas pressure. In their case, the temperature derived from this enhanced loss rate resulted in almost a factor of 2 increase with respect to the experimental trap temperature.

These differences between the measurements and the expected results from the simulation are significant enough to prevent the derivation of the energy distribution from the extraction data. There are multiple potential causes for this disagreement. First and foremost is the possible presence of patch potentials and stray fields due to manufacturing imperfections changing the extraction process, either through the distortion of the ring electrode barrier or simply by affecting the motion or energy of the trapped ions. Limitations in the simulation,

such as the usage of the ideal multipole expression for the rf field, could also play a role. The inefficient motion coupling derived from the simulations seems to be reinforced by the different experimental results at 1 and 300 ms integration, but a more effective coupling may also account for these together with the MCS time-resolved measurements, instead of, or together with the proposed effect of residual buffer gas pressure. An increased efficiency of the motion coupling of the ions was also proposed by Nötzold *et al.* [1] to explain the comparable effect of rf heating measured along the axial and radial directions of their wire trap. We have also assumed through this work that the increased ring electrode voltage has no effect on the experiment other than the increase of the potential barrier in the trap. However, it is possible that the focusing of the ions escaping the trap is dependent on the V_{R4} potential in the subsequent ion optics, affecting their overall detection efficiency. Ultimately, the use of this technique for thermometry measurements requires, effectively, an accurate knowledge of the potential inside the trap, especially the ring electrode barrier, and, potentially, an experimental calibration of this barrier using ions of known energy might be a better suited approach to refine the energy sampling method. This may be accomplished by launching ions directly from the SIS into the trap and stopping them with either the ring or exit electrodes, providing a relation between both potentials. Another possibility is to use a process with well known energetics, such as the quenching of an excited ion state in a LOS experiment, to calibrate the barrier.

Despite these caveats, the proposed energy sampling

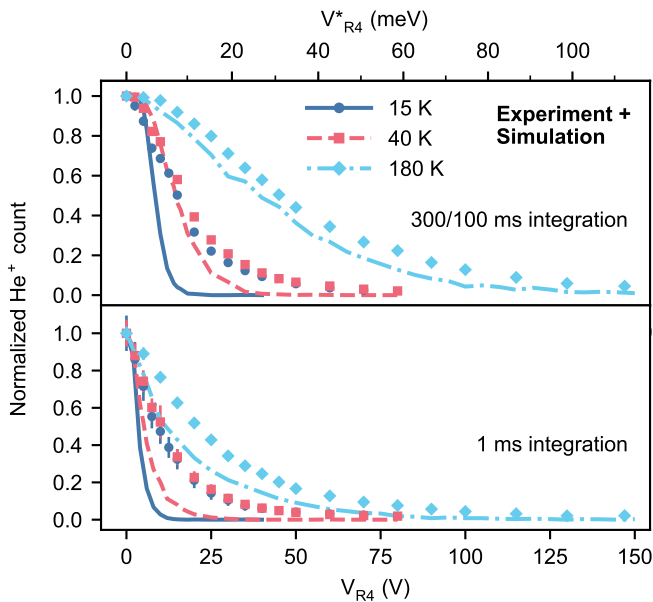


FIG. 8. Comparison of experimental and simulated number of extracted ions as a function of V_{R4} voltage for different trap temperatures. Symbols represent experimental data, lines correspond to simulation results. The experimental trap temperature values are 17, 36 and 180 K respectively (only three sets of data are plotted for clarity). Upper panel: long integration time (300 ms for experimental data, 100 ms for simulations). Lower panel: 1 ms integration time. Simulation results correspond to a residual gas pressure of 2×10^{-6} mbar (see text).

setup is still proven to reliably distinguish between ion distributions with characteristic energies that differ by tens of meV. Furthermore, the effect of the collisions with neutral gas is found to be confined to long integration times, meaning that, in principle, the results of this sampling method should be consistent even with some pressure present in the trap, as long as the characteristic collisional time is larger than the short-scale sampling window. This opens up the possibility of using this method to study a variety of ion-molecule processes in the trap, such as the energetics of exothermic ion-molecule reactions.

An example of one such measurement is shown in Fig. 9. Energy sampling experiments were conducted for H_3^+ ions produced in different ways and at different trap temperatures. Ions that were produced in the Storage Ion Source (SIS) (in the same way as the He^+ presented above) present extraction curves depending on their temperature, with a behavior that is quite similar to the He^+ experiments. A markedly different result is obtained when the H_3^+ ions are produced inside the trap. In this case, H_2^+ ions are stored in the trap together with a very low number density ($\sim 1 \times 10^9 \text{ cm}^{-3}$) of neutral H_2 gas, so that H_3^+ is produced through the 1.7 eV exothermic reaction $H_2^+ + H_2 \rightarrow H_3^+ + H$. A fraction of the energy released ends up as translational energy of

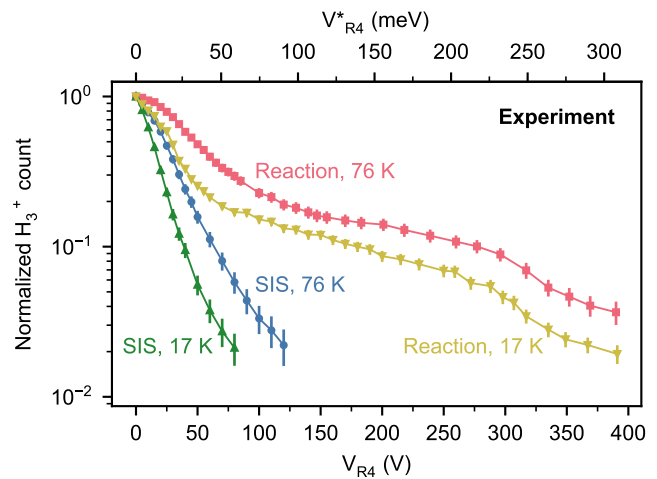


FIG. 9. (Color online) Experimental number of H_3^+ ions extracted as a function of the V_{R4} voltage for two different trap temperatures and production methods. Blue circles and green upward triangles: H_3^+ ions produced in the Storage Ion Source (SIS) and subsequently trapped. Red squares and yellow downward triangles: H_3^+ ions created in the trap through the exothermic reaction $H_2^+ + H_2 \rightarrow H_3^+ + H$. Integration times are 300 ms for all measurements.

the H_3^+ ion, which is clearly visible in the experiment, as the ring electrode voltages needed to contain the ions inside the trap are ~ 3 –4 times larger than for thermal ions. Secondary processes, such as the quenching of the vibrationally excited ions produced in the reaction, will also contribute to this increased high kinetic energy tail. This makes the extraction of precise information about the energetics of the reaction quite challenging and will be the subject of future work. Furthermore, collisions with the neutral gas are a necessary part of the experimental procedure, and, as seen before, these collisions hinder the recovery of the energy distribution information from the extraction curve. Nevertheless, the very clear effect of the exothermic process on the experimental results suggests that the distinction of ions of the same mass produced in the trap, as is the case with reactions producing different isomers (with different exothermicity, i. e., kinetic energies), can be achieved with this technique. Although we clearly demonstrate that our method is sensitive even below 40 K for He^+ , we expect further experimental optimization will be required in order to study processes involving $< 4 m/z$ ions, like the proton exchange $H^+ + H_2(o) \rightarrow H^+ + H_2(p)$ leading to the *ortho* to *para* conversion of the hydrogen molecule [33], with exoergicity as low as $< 15 \text{ meV}$ ($< 175 \text{ K}$).

V. SUMMARY AND CONCLUSIONS

We present an experimental method for the characterization of ion energies in a 22-pole trap using ring electrodes. By inducing small potential barriers before the

trap exit, the trapped ions can be selectively extracted depending on their energy and subsequently detected. The experimental investigation of this method has been complemented by numerical simulations in order to identify the role of various processes, such as ion motion coupling or residual buffer gas collisions, in the expected results.

He^+ ions have been confined at different trap temperatures and subsequently sampled in order to test the experimental method, obtaining different curves for the extracted ion fraction as a function of the applied ring electrode voltage. These curves, which can be likened to energy distributions, are observed to get narrower (i. e., trend towards lower energies) as the trap temperature is decreased. Comparison of the experimental and simulated time-resolved ion detection suggests that residual buffer gas in the trap may play a role in the extraction process. The energy sampling measurements show discrepancies with the simulations that may be caused by differences between the simulated and real trap potentials or a more efficient motion coupling of the ions than the one predicted in the model. While these discrepancies prevent the derivation of the energy distribution from the extraction data, an experimental calibration of the potential barrier may suffice to refine the energy sampling method.

The method as presented is nevertheless proven to reliably discriminate between ion distributions with characteristic energies that differ by tens of meV, and thus, we expect this energy sampling method to be useful in the study of the energetics of ion-molecule processes in the ion trap, as well as in distinguishing ions in situations where mass spectrometry is not sufficient, such as when dealing with isomers or internally excited species. Another prime target of this method are studies of the energy transfer of internal excitation to translational energy through inelastic collisions, which can consequently directly lead to optimization of the LOS setups [13, 34]. The possibility to modify the ion energy distribution in the trap by selective evaporation puts this technique ahead of other sampling methods relying on either full ejection of the ion cloud [11] or on buffer gas induced evaporation [12]. We have already showcased the usefulness of this method in highly exothermic ion-molecule reactions, by distinguishing ions created in the trap from those produced in the Storage Ion Source.

The ion trajectory code employed in this work can be readily extended to include reactive collisions in which the nascent ions gain high kinetic energies, either from the exothermicity of the reaction, or from internal degrees of freedom, e. g., induced by absorbed photon, supporting our future experimental work focused on processes between ions and neutrals at astrophysically relevant conditions. We intend to explore the possible broadening of the method towards mass spectrometry inside the trap, i. e., trap and ring electrode configuration in which ions are selectively ejected according to their m/z , first computationally (code extensions), then followed by the ex-

periment.

Data Availability

The supporting data for this article are openly available from the zenodo archive DOI: [10.5281/zenodo.8321098](https://doi.org/10.5281/zenodo.8321098).

ACKNOWLEDGMENTS

This work was supported by the Max Planck Society. The authors gratefully acknowledge the work of the electrical and mechanical workshops and engineering departments of the Max Planck Institute for Extraterrestrial Physics. We thank Prof. Stephan Schlemmer for helpful discussions. We thank the Lorentz Center, Leiden, the Netherlands for organising the “New Directions in Cold and Ultracold Chemistry” workshop and its participants for fruitful discussions.

Appendix A: Coupling of the ion motion

The ion motion is dominated by the effective potential V^* (see Fig. 1), which governs the macromotion of the ions. Accordingly, the possible coupling of the different degrees of freedom will be determined by the interaction of the ions with this potential.

The effective potential created by an ideal multipole of order n as a function of the radial coordinate r scales as $V^* \propto r^{2n-2}$ (see for instance [25]). As a consequence, a significant fraction of a 22-pole trap volume is virtually a field free region, which is one of the advantages of this design. Close to the poles, however, this potential grows very rapidly. As a consequence, ions moving towards the poles are essentially reflected by this effective potential and should retain their energy distribution across the different degrees of freedom.

In a real trap, however, the end electrodes and ring electrodes will also contribute to the effective potential. In the central region, sufficiently far from the ends, their contribution is small (see Fig. 1 and [24]) and the assumptions of the previous paragraph for radial motion should hold. The situation gets more complicated for the axial motion. The potential does not grow as fast in that direction compared to the radial one, and there is a weak dependence also along the radial direction for a given axial coordinate. It can then be expected that, as the ions change trajectory due to this potential, some of the deflections result in a transfer of kinetic energy between the different degrees of freedom. This effect should be particularly relevant if the ion moves towards the corners of the trap, where the contributions of both end electrodes and poles are significant. How often this transfer of energy happens will likely depend on the particular ion motion

and the electrode configuration and can be better examined in our simulations.

An example of the motion of a single trapped ion moving according to the effective potential of the trap is shown in Fig. 10. The time evolution of the kinetic energy (E_k) and the contribution from the different degrees of freedom (radial, r , angular, φ , and axial, z) in a sub-ms timescale is shown in the upper panel and its trajectory in the xz , xy planes in panel A. As the ion moves inside the trap, it bounces back and forth due to the confining field, producing the oscillatory behavior observed for the kinetic energy. These oscillations are nevertheless found to have regular amplitudes as seen from the almost constant envelopes obtained from the respective maxima, meaning that the ion is not exchanging kinetic energy between the different degrees of freedom at \ll ms timescales. Several distinctive motion patterns, with distinctive E_k components, have been identified (A–C). A particular ion may change the motion pattern, even without undergoing a collision with a neutral.

Since the axial kinetic energy controls whether the ion is able to escape the trap, the potential coupling of the energy in the different degrees of freedom for the motion of the ion will play a significant role in the sampling process. This is examined in Fig. 11. The left panel expands the results of Fig. 10 to a 1 ms interval, and still, no significant exchange between the different kinetic energy contributions can be observed, i. e., within this time frame only the initial axial velocity and potential energy will play a role in the extraction of the ion. For longer timescales, however, the situation changes dramatically, as seen in the right panel of Fig. 11. Along the 100 ms simulation, the maximum kinetic energy in the axial direction varies significantly, accounting for a minimum of 1.6 meV to a maximum of 4.6 meV of the total ion energy of 5.4 meV. This implies that the coupling between different E_k components is possible in this timescale and an ion can escape the trap long after the start of the simulation if its axial kinetic energy becomes higher than the V_{R4}^* potential barrier.

For a complete description of this coupling, the effect of the micromotion caused by the rf field should also be considered. The analysis of the ion kinetic energy, however, becomes much more complex in this case, as the ions gain large amounts of energy when moving closer to the rods where the rf field is stronger. This means that it is no longer possible to examine the coupling of the motion by simply looking at the kinetic energy envelopes as in Fig. 11.

Nevertheless, the behavior observed for the axial energy $E_{k,z}$, which is not affected by this micromotion, is similar to the one in the effective potential simulations. This fact, coupled with the similar results of the energy sampling simulations performed using the effective potential and the time-dependent rf field, suggests that the micromotion is not a major factor in the coupling of the different degrees of freedom.

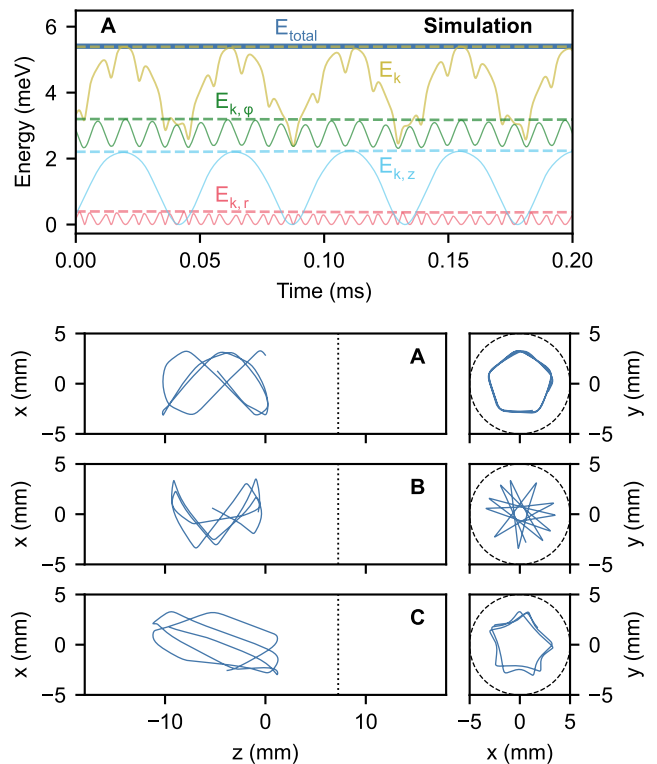


FIG. 10. (Color online) Upper panel: simulated time evolution of the total kinetic energy (E_k , yellow) and the kinetic energy for the different degrees of freedom, radial ($E_{k,r}$, red), angular ($E_{k,\varphi}$, green) and axial ($E_{k,z}$, cyan), along with the total energy (sum of kinetic and potential, bold blue line), for a trapped He^+ ion from a 15 K distribution residing in the trap with a $V_{R4} = 30$ V barrier and no buffer gas collisions, during the first 0.2 ms of the simulation (time A). Dashed lines represent an envelope obtained from the maximum values of the different energies in 0.1 ms bins. Lower panels: projection of the ion trajectory during 0.2 ms in the xz and xy planes, for the aforementioned ion at three different times of the 100 ms simulation, A, B, C, corresponding to motion dominated by angular, radial, and axial velocities respectively (see Fig. 11 for details). The vertical dotted line represents the position of the ring electrode barrier, the circular dashed line shows the inscribed radius r_0 of the 22 rods.

Appendix B: Detailed energy sampling analysis

The experimental and simulation results for the energy sampling can be further analyzed by using the value of the V_{R4} voltage at which the fraction of extracted ions is 0.5 ($V_{0.5}$) and 0.1 ($V_{0.1}$). These are collected in Table I, including those for the 75 and 100 K data omitted in Fig. 8. For the long integration times, the values of $V_{0.5}$ are reasonably well reproduced by the simulations, except at 15 K, but the $V_{0.1}$ values are consistently underestimated, meaning the higher barrier values can be overcome by a larger amount of ions than expected from the simulations. At 1 ms the discrepancy is much larger, with the experimental $V_{0.5}$ values almost doubling those

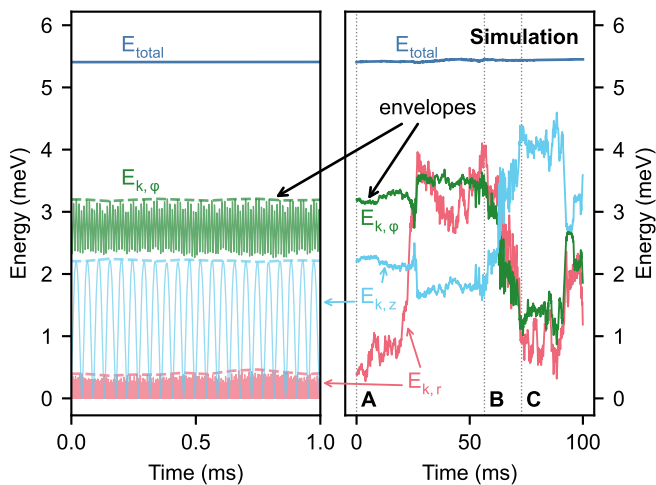


FIG. 11. Simulated coupling of the kinetic energy in the different degrees of freedom, radial ($E_{k,r}$, red), angular ($E_{k,\phi}$, green) and axial ($E_{k,z}$, cyan), along with the total energy (sum of kinetic and potential, bold blue line) for the same ion trajectory depicted in Fig. 10. Left panel: time evolution during the first ms (solid lines), along with the envelopes obtained from the maximum values (dashed lines). Right panel: time evolution for the full 100 ms simulation, using the aforementioned envelopes for clarity. The dotted vertical lines show the times A, B and C corresponding to the trajectory plots in Fig. 10. Note that there are no collisions, i. e., the ion motion, and the coupling between the E_k components, is governed solely by the effective potential.

obtained from the simulations, and $V_{0,1}$ voltages that diverge particularly at the lower temperatures. Despite the 1 ms integration time largely sidestepping the effect of collisions with the neutral gas, it is unclear whether that introduces additional issues in the sampling processes leading to the observed discrepancies.

-
- [1] M. Nötzold, R. Wild, C. Lochmann, and R. Wester, *Physical Review A* **106**, 023111 (2022).
- [2] R. Plašil, L. Uvarova, S. Rednyk, Štěpán Roučka, E. Vanko, P. Dohnal, and J. Glosfík, *The Astrophysical Journal* **948**, 131 (2023).
- [3] E. S. Endres, G. Egger, S. Lee, O. Lakhmanskaya, M. Simpson, and R. Wester, *Journal of Molecular Spectroscopy* **332**, 134 (2017).
- [4] P. Jusko, O. Asvany, A.-C. Wallerstein, S. Brünken, and S. Schlemmer, *Phys. Rev. Lett.* **112**, 253005 (2014).
- [5] S. Brünken, L. Kluge, A. Stoffels, J. Pérez-Ríos, and S. Schlemmer, *Journal of Molecular Spectroscopy* **332**, 67 (2017).
- [6] M. Nötzold, S. Z. Hassan, J. Tauch, E. Endres, R. Wester, and M. Weidemüller, *Applied Sciences* **10**, 5264 (2020).
- [7] H. J. Williams, S. Truppe, M. Hambach, L. Caldwell, N. J. Fitch, E. A. Hinds, B. E. Sauer, and M. R. Tarbutt, *New Journal of Physics* **19**, 113035 (2017).
- [8] W. Alt, D. Schrader, S. Kuhr, M. Müller, V. Gomer, and D. Meschede, *Phys. Rev. A* **67**, 033403 (2003).
- [9] Z. Hua, S. Feng, Z. Zhou, H. Liang, Y. Chen, and D. Zhao, *Review of Scientific Instruments* **90**, 013101 (2019).
- [10] M. D. Johnston, W. L. Pearson, III, G. Wang, and R. B. Metz, *Review of Scientific Instruments* **89**, 014102 (2018).
- [11] R. J. Champeau, A. Crubellier, J. O. Gaardsted, D. Marescaux, and D. Pavolini, *Journal of Physics B: Atomic, Molecular and Optical Physics* **27**, 905 (1994).
- [12] O. Y. Lakhmanskaya, T. Best, S. S. Kumar, E. S. Endres, D. Hauser, R. Otto, S. Eisenbach, A. von Zastrow, and R. Wester, *International Journal of Mass Spectrometry* **365–366**, 281 (2014).
- [13] P. C. Schmid, O. Asvany, T. Salomon, S. Thorwirth, and S. Schlemmer, *The Journal of Physical Chemistry A* **126**, 8111 (2022).
- [14] G. B. Andresen, M. D. Ashkezari, M. Baquero-Ruiz, W. Bertsche, P. D. Bowe, E. Butler, C. L. Cesar, S. Chapman, M. Charlton, J. Fajans, T. Friesen, M. C. Fujiwara, D. R. Gill, J. S. Hangst, W. N. Hardy, R. S. Hayano, M. E. Hayden, A. Humphries, R. Hydromako, S. Jonesell, L. Kurchaninov, R. Lambo, N. Madsen, S. Menary, P. Nolan, K. Olchanski, A. Olin, A. Povilus, P. Pusa, F. Robicheaux, E. Sarid, D. M. Silveira, C. So, J. W. Storey, R. I. Thompson, D. P. van der Werf, D. Wilding, J. S. Wurtele, and Y. Yamazaki (ALPHA Collaboration), *Phys. Rev. Lett.* **105**, 013003 (2010).
- [15] J. Tauch, S. Z. Hassan, M. Nötzold, E. S. Endres, R. Wester, and M. Weidemüller, *Nat. Phys.* **19**, 1270 (2023).
- [16] R. G. DeVoe, *Physical Review Letters* **102**, 063001 (2009).
- [17] O. Asvany and S. Schlemmer, *International Journal of Mass Spectrometry* **279**, 147 (2009).
- [18] G. Rajeevan, S. Mohandas, and S. S. Kumar, *Physica Scripta* **96**, 124001 (2021).

TABLE I. Voltages at which the fraction of ions extracted falls to 0.5 ($V_{0.5}$) and 0.1 ($V_{0.1}$) for the experimental (Exp) and simulation (Sim) data presented in Figs. 3, 7 and 8, depending on the integration time. Simulation results correspond to a residual gas pressure of 2×10^{-6} mbar (see text).

T (K)		300/100 ms				1 ms			
		$V_{0.5}$ (V)		$V_{0.1}$ (V)		$V_{0.5}$ (V)		$V_{0.1}$ (V)	
Exp	Sim	Exp	Sim	Exp	Sim	Exp	Sim	Exp	Sim
17	15	15.1 ± 0.4	8.5	28.9 ± 1.4	12.9	9.2 ± 1.9	3.5	30.8 ± 5.1	7.3
36	40	17.1 ± 0.4	14.6	42.0 ± 1.2	26.2	10.6 ± 2.4	5.2	32.2 ± 3.6	13.1
76	75	22.7 ± 0.8	21.7	56.9 ± 1.9	40.1	11.8 ± 1.2	7.5	34.7 ± 3.2	22.2
107	100	31.3 ± 2.0	26.0	81.7 ± 6.0	52.2	14.4 ± 2.2	8.5	49.0 ± 8.5	27.5
180	180	45.4 ± 1.2	39.3	110.8 ± 2.7	85.5	21.0 ± 1.5	11.6	68.4 ± 4.7	47.9

- [19] B. Höltkemeier, P. Weckesser, H. López-Carrera, and M. Weidemüller, *Physical Review Letters* **116**, 233003 (2016).
- [20] B. Höltkemeier, P. Weckesser, H. López-Carrera, and M. Weidemüller, *Physical Review A* **94**, 062703 (2016).
- [21] A. Svendsen, L. Lammich, J. E. Andersen, H. K. Bechtold, E. Søndergaard, F. Mikkelsen, and H. B. Pedersen, *Physical Review A* **87**, 043410 (2013).
- [22] H. A. Fürst, N. V. Ewald, T. Secker, J. Joger, T. Feldker, and R. Gerritsma, *Journal of Physics B: Atomic, Molecular and Optical Physics* **51**, 195001 (2018).
- [23] E. Trimby, H. Hirzler, H. Fürst, A. Safavi-Naini, R. Gerritsma, and R. S. Lous, *New Journal of Physics* **24**, 035004 (2022).
- [24] P. Jusko, M. Jiménez-Redondo, and P. Caselli, *Molecular Physics* **122**, e2217744 (2024).
- [25] D. Gerlich, in *Advances in Chemical Physics* (John Wiley & Sons, Ltd, 1992) pp. 1–176.
- [26] W. C. Swope, H. C. Andersen, P. H. Berens, and K. R. Wilson, *The Journal of Chemical Physics* **76**, 637 (1982).
- [27] R. D. Ruth, *IEEE Transactions on Nuclear Science* **30**, 2669 (1983).
- [28] W. Śmigaj, T. Betcke, S. Arridge, J. Phillips, and M. Schweiger, *ACM Transactions on Mathematical Software* **41**, 6:1 (2015).
- [29] T. Betcke and M. W. Scroggs, *Journal of Open Source Software* **6**, 2879 (2021).
- [30] Salome platform, <https://www.salome-platform.org/>.
- [31] F. A. Londry, R. L. Alfred, and R. E. March, *Journal of the American Society for Mass Spectrometry* **4**, 687 (1993).
- [32] C. Tsallis, *Journal of Statistical Physics* **52**, 479 (1988).
- [33] D. Gerlich, *The Journal of Chemical Physics* **92**, 2377 (1990).
- [34] M. Bast, J. Böing, T. Salomon, S. Thorwirth, O. Asvany, M. Schäfer, and S. Schlemmer, *Journal of Molecular Spectroscopy* **398**, 111840 (2023).